JES Focus Issue on Electrocatalysis — In Honor of Radoslav Adzic

Structure–Activity/Stability Correlations from the Electrochemical Dynamic Responses of Titanium Anode Coatings Formed of Ordered TiO_2@RuO_2 Microspheres

Milica Košević,[1] Nataša Vukićević,[1] Srećko Stopić,[2] Jasmina Stevanović,[1,3] Bernd Friedrich,[2] Vladimir Panić,[1,3,4,z] and Branislav Nikolić[5,z]

[1] *Institute of Chemistry, Technology and Metallurgy, Department of Electrochemistry, University of Belgrade, Belgrade, Serbia*
[2] *IME Process Metallurgy and Metal Recycling, RWTH Aachen University, Aachen, Germany*
[3] *Centre of Excellence in Environmental Chemistry and Engineering - ICTM, University of Belgrade, Belgrade, Serbia*
[4] *State University of Novi Pazar, Chemical-Technological Department, Novi Pazar, Serbia*
[5] *Faculty of Technology and Metallurgy, University of Belgrade, Belgrade, Serbia*

Spherical TiO_2/RuO_2 particles were synthesized by ultrasonic spray pyrolysis (USP) at 200 and 800°C. The activity for the oxygen and chlorine evolution reactions (OER and CER, respectively) and the dynamic responses from electrochemical impedance spectroscopy (EIS) of the USP powders, as well as of the corresponding coatings on Ti, were analyzed and are discussed. The loss of coating activity is discussed with respect to the differences in the EIS and cyclic voltammetry responses of the coatings in their active and inactive states. The 800°C-USP sample was found to be more active than the 200°C-USP sample for both the CER and the OER, whereas the stability of the former was considerably lower. The correlation between the structure, composition and morphology of the powder and the coating with the registered electrochemical properties is discussed. The EIS analysis of the coating resistance distributions induced by the thermal treatment of the powder indicated a complex combination of the pore resistance and the pseudocapacitive charge transfer resistance. An additional coating resistance, due to loose grain boundaries, was introduced into the coatings in their active and inactive state. The EIS analysis indicated the changes in TiO_2-enriched core/RuO_2-enriched shell structure, caused by the USP temperature.

 [DOI: 10.1149/2.0521815jes]

Manuscript submitted July 27, 2018; revised manuscript received November 14, 2018. Published November 30, 2018. *This paper is part of the JES Focus Issue on Electrocatalysis — In Honor of Radoslav Adzic.*

The definitions of simple synthesis routes and reliable characterization tools in the pursuit of the rational design of the structure of an electrocatalyst are the main challenges of modern electrochemical investigations.[1] The distribution of the components in an electroactive material consisting of an interactive and cheap support decorated by, as a rule, expensive noble metal-based carrier(s) of the activity appears crucial for the activity and stability of an electrode assembly of a given composition.[2] The core@shell hierarchy[3,4] of a catalyst monolayer encapsulating a nanoparticle is envisaged as the limiting rationalization of the structure for high stability/lowest catalyst content.

Besides Pt-based catalysts for both oxidation[5] and oxygen reduction reactions[6] of importance in fuel cells and batteries, noble metal-based porous electrode materials for industrial electrochemical processes also require fine tuning of activity–stability–structure. The TiO_2/RuO_2 binary and the electrochemically more stable TiO_2/RuO_2–IrO_2 ternary oxide are so far the best electrocatalysts for gas-evolving anodic reactions.[7] Ti anodes with coatings of these oxide mixtures are widely used for the industrial production of chlorine[8–10] and as the oxygen-evolving anodic counterpart in water splitting, the direct or indirect electrochemical degradation of organic contaminants in waste water treatment, the electrowinning of metals, cathodic protection, etc.[10–13]

It is known that the preparation conditions influence considerably the morphology and microstructure of a Ti anode coating, and consequently, its electrochemical behavior as a catalyst.[14–17] Novel synthetic routes to generate ultrafine particles of TiO_2/RuO_2 mixed metal oxides were applied to meet the requirement for significant improvement of the electrocatalytic activity.[18–20] Core@shell arrangements are reported for RuO_2@IrO_2[21] and TiO_2@RuO_2.[22] A simple solvatothermal plating of RuO_2 by IrO_2 produced RuO_2@IrO_2 of improved activity toward the oxygen evolution reaction (OER), with respect to the individual oxides.[21] DFT calculations indicated that the improvement of the activity was due to the slightly reduced adsorption strength of O-based reaction intermediates. The calculations also predicted that TiO_2 could be more suitable oxide core than RuO_2, for good OER activity. Another synthesis approach to generate sub-μm, almost ideally spherical, TiO_2 core–RuO_2 shell particles has been presented.[22] The approach was based on the sequential ultrasonic spray pyrolysis (USP) method. The oxide aerogels, separately-formed by high-frequency ultrasound, were joined in a subsequent spray pyrolytic step. This resulted in the formation of 300-nm TiO_2 cores encapsulated in a few tens of nm thick RuO_2 shell.

Most recently, the coupled single-step USP/electrostatic coating deposition setup was applied for the generation of a USP RuO_2/TiO_2 coating onto expanded titanium.[23] The coating, which can also be prepared on Ti from a USP powder suspension, exhibited typical electrochemical properties of activated titanium anodes (ATAs).[15,24,25] The USP-obtained ATA was found highly stable in brine electrolysis if the pyrolysis temperature was rather low (200°C)[26] with respect to typical coating formation temperatures (450–500°C).[24,27,28] When the nominal pyrolysis temperature was increased to extremely high for full conversion of precursors to oxides (800°C), the coating stability considerably deteriorated.[23,26] At both low and high temperature extremes, the structure of the native RuO_2-encapsulated TiO_2 spheres was, however, well preserved in the final ATA coating. USP is thus introduced as a synthesis route allowing full coating texture control in the penultimate step of the mixed oxide formation. Although the core/shell hierarchy is not fully confirmed in non-sequential, single-step USP, the electrochemically active surface area of a (60 mol %) RuO_2/(40 mol %) TiO_2 powder synthesized at a higher USP temperature was similar to that of pure RuO_2.[26] This indicated that the properties of TiO_2 spheres resemble RuO_2, which makes a compact sphere shell, i.e., the specific activity of RuO_2 increased in the USP-synthesized RuO_2/TiO_2.

It follows that the USP synthesis approach is suitable for an analysis of electrocatalytically active oxides since the TiO_2/RuO_2 powders of defined and stable structure are formed by USP. Furthermore, the

[z]E-mail: panic@ihtm.bg.ac.rs; bane@tmf.bg.ac.rs

electrochemical investigation can be performed in the form of either a thin layer on an appropriate current collector (e.g., glassy carbon) or a coating on a Ti substrate. For the latter, the coating procedure requires a final thermal treatment at 450°C,[23,26] in order to attain good coating adhesion. In an introductory investigation, the thermal treatment was found disadvantageous, since the electrochemically active surface area of the initial USP powder was considerably decreased.[26] As a result, the voltammetric behaviors of the coatings obtained at the two USP temperature extremes did not differ considerably, but their stabilities did. The preliminary ac impedance analysis showed that these two coatings had considerably different distributions of the active sites and pore resistance throughout the coating.[26] The active sites of the coating obtained with the low USP temperature were uniformly distributed along with a much more pronounced pore resistance and distribution with respect to the high USP temperature sample with the active sites being located mostly in the interiors of the coating. These internal active sites are, however, accessible through lower pore resistance. The registered differences in the coating depth-dependent activity and the structure caused by USP temperature, which caused considerable difference in stability, are to be investigated further in order to unambiguously define the mechanism of the loss of coating activity.

The main aim behind this work, in continuation of a previous investigation,[26] was to reach full correlation between the separately analyzed electrochemical performances of the USP powders and the corresponding coatings on Ti. An appropriate comparison of the results obtained from the voltammetric characterization and the polarization of the coatings in oxygen and chlorine evolution reactions, as well as the ac impedance responses of the powders and coatings in active and inactive states was performed. Structure–activity/stability correlations are discussed to elucidate the causes of the apparently opposing findings for the activities of powders and stabilities of the coatings prepared at the two USP temperature extremes (200 and 800°C).[23,26]

Experimental

The TiO_2/RuO_2 powders were synthesized by USP at 200°C, TiO_2/RuO_2(200), and at 800°C, TiO_2/RuO_2(800), as described previously in detail.[23] Tetra-*n*-butyl orthotitanate and ruthenium(III) chloride hydrate in hydrochloric acid solution were driven by an O_2 flow through a tube furnace pre-heated to the desired temperatures upon aerosol generation by ultrasonic atomization (2.5 MHz). The final calcinations were performed during powder collection on an electrostatic mesh filter (30 kV, 0.08 mA) at 120 and 500°C for TiO_2/RuO_2(200) and TiO_2/RuO_2(800), respectively. The coatings on a Ti substrate (rods, 3 mm in diameter) were formed from TiO_2/RuO_2 powders, ultrasonically suspended in 2-propanol.[26] The suspensions were brushed over Ti rods in 6 layers. The deposition of each layer consisted of the drying of the brushed suspension at 120°C and subsequent annealing at 450°C for 5 min. Upon reaching a coating amount of 1 mg cm^{-2}, the anodes were finally annealed at 450°C for 20 min.

The electrochemical response of synthesized TiO_2/RuO_2 powders was gained from their thin layer formation on a GC support. The GC-supported layer of 0.31 mg RuO_2/TiO_2 per cm^2 of a GC disc was formed from 3 mg/mL powder suspensions. The suspensions were prepared in water from as-synthesized TiO_2/RuO_2(800) powder, air-dried at 120°C for 24 h or from TiO_2/RuO_2(800) and TiO_2/RuO_2(200) powders, thermally-treated at 450°C for 30 min. The thermal treatments were performed in order to check the influence of the thermal regime on the properties of the USP-synthesized mixed oxides, as will be applied during the coating preparation. Good adhesion of a layer on GC was ensured by covering the room-dried layer with Nafion (from 1:100-diluted solution of 10 mass% Nafion).

The cyclic voltammetry (CV) and electrochemical impedance spectroscopy (EIS) measurements were performed in 1.0 M H_2SO_4 and 5 M NaCl, pH 2, in a three-electrode electrochemical cell with GC-supported layers or TiO_2/RuO_2/Ti anodes as working electrodes, a saturated calomel electrode as the reference and a Pt plate as the counter electrode. CV was performed at a sweep rate of 50 mV s^{-1}. The electrochemical performances of the coatings were further investigated for their activity in the chlorine (from 5 M NaCl, pH 2) and the oxygen (from 1.0 M H_2SO_4) evolution reactions by anodic linear low sweep rate (2 mV s^{-1}) voltammetry (ALSV). The EIS measurements were conducted on as-prepared coatings and after their degradation by an accelerated stability test (AST).[23,26] Since different mixed oxide compositions were found for the TiO_2/RuO_2(200) and TiO_2/RuO_2(800) coatings (TiO_2/RuO_2 mass ratios of 3:2 and 2:3 were found, respectively[26]), another coating with the composition adjusted to that of TiO_2/RuO_2(200) by the addition of $TiCl_3$ into the TiO_2/RuO_2(800) powder suspension for coating preparation was prepared and tested (TiO_2/RuO_2(800cc)/Ti).

A Bio-Logic SAS potentiostat/galvanostat, model SP-200, was applied to perform the experiments at room temperature. The EIS was recorded with a sinusoidal voltage of 10 mV amplitude, in a multisine mode around spontaneously established open circuit potential before and after the AST. Stable open circuit reading for this type of material can be established in a rather wide potential range covering almost full range of water thermodynamic stability.[29,30] In this range, the dynamic response of the material is almost purely pseudocapacitive. It is believed that open circuit potential could correspond to several fast redox transitions of Ru species, with typical values around 0.5 V_{RHE} (from 0.2 to 0.8 V, depending on pH).[31] Consequently, the readings correspond to the pure pseudocapacitive response. These considerations suggest that stable pseudocapacitive EIS response should be rather recorded in a freely established equilibrium state, i.e., at open circuit potential, than at some fixed arbitrary potential value, especially due to different coating state induced by AST.

ZView, version 3.2b, software from Scribner Associates Inc. was applied to fit the registered EIS data. Since the data were registered as capacitive-like response, they were fitted into the time constants-distributed electrical circuit of resistor and capacitor in series,[32] i.e., the transmission line equivalent electrical circuit (TLEEC, $R_\Omega(C_0(R_{p,1}(C_1(R_{p,2}(\ldots(R_{p,n}C_n)))\ldots)$, where C_n relates to the capacitance in series to $\sum_{i=1}^{n} R_{p,i}$ resistances; R_Ω relates to electrolyte ohmic resistance).[12,33] The appropriate, most reliable, TLEEC was chosen according to the values of several fitting quality parameters. TLEEC was required to return the lowest possible standard deviation (*SD*) of the values of circuit parameters and overall *SD* of circuit error for as low as possible χ^2 and weighted sum of squares. Additionally, relative deviation of TLEEC data from measured data was also checked. The details related to the choice of appropriate TLEEC and corresponding fitting quality data are given as Supplementary material to this paper. The fitting data were analyzed as the distributions of capacitances and the coating resistances along the branches of the TLEEC. The number of required circuit elements was different, which is indicated as different ranges of "Branch No." (*n*) axis of the capacitance and pore resistance distribution plots.

Results and Discussion

The activity for chlorine and oxygen evolution reactions.—The polarization data of the USP coatings on Ti for the chlorine (CER) and for the oxygen evolution (OER) reactions are shown in Fig. 1. Differences in both the Tafel slopes and the currents were registered. The coatings are of the typical slopes close to 40 mV for CER,[7,10,34] with a bit higher value for the high USP temperature sample. This low-activity feature appears to be caused by the richer RuO_2 composition of TiO_2/RuO_2(800). The data for the coating with the adjusted composition approach the data for the coating obtained at the low USP temperature. The adjustment of the coating composition additionally caused an increase in the currents, even above those for TiO_2/RuO_2(200)/Ti. These benefits of added TiO_2 were also found for the OER in the high-overpotential region: the limiting current-like behavior of TiO_2/RuO_2(800)/Ti transfers to the appearance the 120 mV Tafel slope of TiO_2/RuO_2(800cc)/Ti, which is more similar to the usual OER kinetics considerations.[35,36] The typical change in the Tafel slope from 60 to 120 mV was also found for TiO_2/RuO_2(200)/Ti.

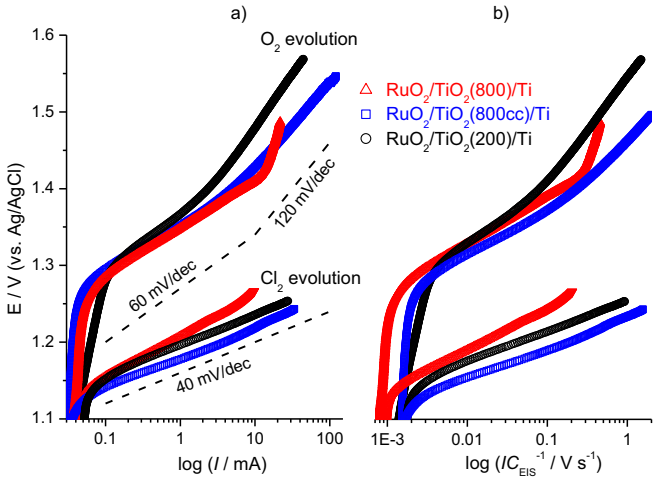

Figure 1. a) *IR*-corrected polarization data of the prepared USP coatings on Ti in their active states (before AST) registered in 1.0 M H_2SO_4 and 5 M NaCl, pH 2; b) the curves with the registered currents divided by the total coating capacitance obtained from EIS measurements.

Besides lower OER activity, the region with the lower Tafel slope at low overpotentials is shorter, in comparison to that of the high USP temperature samples.

The registered characteristics indicate the difference in electrocatalytic properties between the mixed oxides synthesized at different temperatures, which cannot to be assigned only to the differences in electrochemically active surface area, the availability of active sites and the coating morphology, i.e., "geometric" factors, but also to different oxide structures and surface states ("electronic" factor[7]). Namely, the voltammetric currents[26] showed different trend in comparison to the polarization data. The largest voltammetric charge was exchanged by TiO_2/RuO_2(200)/Ti, which demonstrated only moderate CER and OER activity. The distribution of the pseudocapacitive ability through the coatings, as analyzed by EIS,[26] indicated even more drastic differences in their activities. The capacitance values of the external surface of TiO_2/RuO_2(200)/Ti are by more than two orders of magnitude higher than the corresponding values of TiO_2/RuO_2(800)/Ti and TiO_2/RuO_2(800cc)/Ti. These findings indicate that TiO_2/RuO_2(200)/Ti should be much more active in CER and OER, but this was not the case according to Fig. 1. The normalization by the total coating capacitance (gained by EIS analysis as a measure of the available active surface area) to remove the influence of coating morphology on the measured currents, Fig. 1b, did not considerably affect the initial trend from Fig. 1a.

It is clear from Fig. 1 that the composition-adjusted coating, TiO_2/RuO_2(800cc)/Ti appeared as the most active in both CER and OER (Fig. 1b). The main difference between this and the other two samples could lie in the manner of the introduction of the complete amount of TiO_2. $TiCl_3$ was added to the already USP-formed TiO_2/RuO_2 during the thermal formation of the coating, in order to correct the overall coating composition from 2:3 in the native spheres to 3:2. Bearing in mind the USP-generated structure,[22] it could be assumed that the composition of the coating was most likely changed in the shell, originally consisting of almost pure RuO_2, or even more locally, at the utmost RuO_2 shell surface. The newly generated sphere structures could be of single-, $TiO_2/(RuO_2+TiO_2)$, or double-layered shell, $TiO_2/RuO_2|TiO_2$. Taking into account that the pore resistance in the external parts of the TiO_2/RuO_2(800cc) coating was lower in comparison to that of the TiO_2/RuO_2(800) coating, while the number of active sites was increased, a $TiO_2/(RuO_2+TiO_2)$ structure is more probable, i.e., the two oxides are mixed throughout the shell of the pure TiO_2 core. It is known that TiO_2 in mixed RuO_2+TiO_2[28,37] induces the development of an active surface area and stabilizes RuO_2 during electrolysis. Its presence in the shell could thus result in TiO_2/RuO_2(800cc)/Ti having improved activity and stability when compared to TiO_2/RuO_2(200)/Ti and TiO_2/RuO_2(800)/Ti. However, the external coating activity is still not high enough to compete with the long-lasting TiO_2/RuO_2(200)/Ti.

EIS responses in the service in the consideration the core/shell structure of USP TiO_2/RuO_2 powders.—To determine the proving details related to the structure-related activity/stability considerations, impedance measurements and analysis were performed on the USP-synthesized powder to check the influence of their structure on the behavior of the coating. The registered and fitting EIS data are presented in Fig. 2 selectively as complex plane and phase angle shift plots, where the differences between the powders are the most apparent. Three different states of the TiO_2/RuO_2(800) powder were investigated to follow the changes in the powder during the thermal treatment of the corresponding coating, i.e., USP as-received, dried and calcined state. However, the TiO_2/RuO_2(200) powder required calcinations since the as-received and dried states were not stable in suspensions and/or in electrolyte solution for reliable experiments.[26]

All of the samples showed pseudocapacitive-like behavior, with an increasing contribution of finite diffusion through the porous structure, which was the most pronounced in the case of TiO_2/RuO_2(200). The declination in the impedance complex plane presentation is closest to 45°, while high- to mid-frequency phase shift reach the same value for this sample. The most pronounced feature of the capacitance complex plane plot for this sample is the overlapping of the loops due to similar *RC* time constants. On the other hand, this plot for the as-received TiO_2/RuO_2(800) expresses a well-resolved capacitive loop over a wide frequency range. This suggests that the EIS behavior typical for porous structures[32,38] is considerably less pronounced in the case of as-prepared USP powder, since a porous structure develops in subsequent thermal treatments. It is strange that even moderate drying at 120°C caused significant changes in the shape of the capacitance spectrum, since the related mass loss was only up to 2%.[26] Even more, the complete mass loss did not exceed 4% up to 500°C, while the capacitance of the calcined sample was only 1/10 of that of the as-received sample (the highest imaginary capacitance in Fig. 2).

The quantification of the changes in the powder structure with the thermal treatment, as reflected in the impedance characteristics (Fig. 2), is presented in Fig. 3 as the distributions of the pore resistance and the capacitance through a layer of the powder. The data were gained by fitting the experimental EIS data to an appropriate TLEEC of seven branches of the pore-related resistor and the equivalent material capacitor in series ($n = 7$).

The similarities between the changes in capacitance and resistance distributions caused by drying, which support the above consideration of the structural changes, are as follows. The influence of the water-removal effect reverses at $n = 5$ for both R_p and the C distribution. The shares of the increase in R_p and the decrease in C in preceding branches with respect to the as-prepared powder state are quite similar: 50–55% for the former and 58% for the latter. This introduces a close connection between R_p and C. Hence, if C bears the pseudocapacitive contribution, then R_p relates not only to the pore resistance, but also to the charge transfer resistance, associated with pseudocapacitive redox transitions of the hydrated oxide.[39] As the capacitance decreases/increases through the shell, the overall resistance changes proportionally.

As evident in Fig. 3, the complete dehydration and crystal structure formation should occur upon calcination. The capacitance at all shell levels decreases considerably (except at the point related to the size of the spheres, $n = 0$ as discussed), roughly by an order of magnitude, while, again proportionally, R_p increases. This additionally supports the considerations about the subtle structural changes in the shell. In addition, the development of the porous structure on thermal treatments, as discussed in relation to Fig. 2, should then be assigned to the causes related rather to structural changes than to the changes in the pore geometry and morphology.

Another important finding is that distributions for TiO_2/RuO_2(800) and TiO_2/RuO_2(200) in the calcined state are similar. The observed

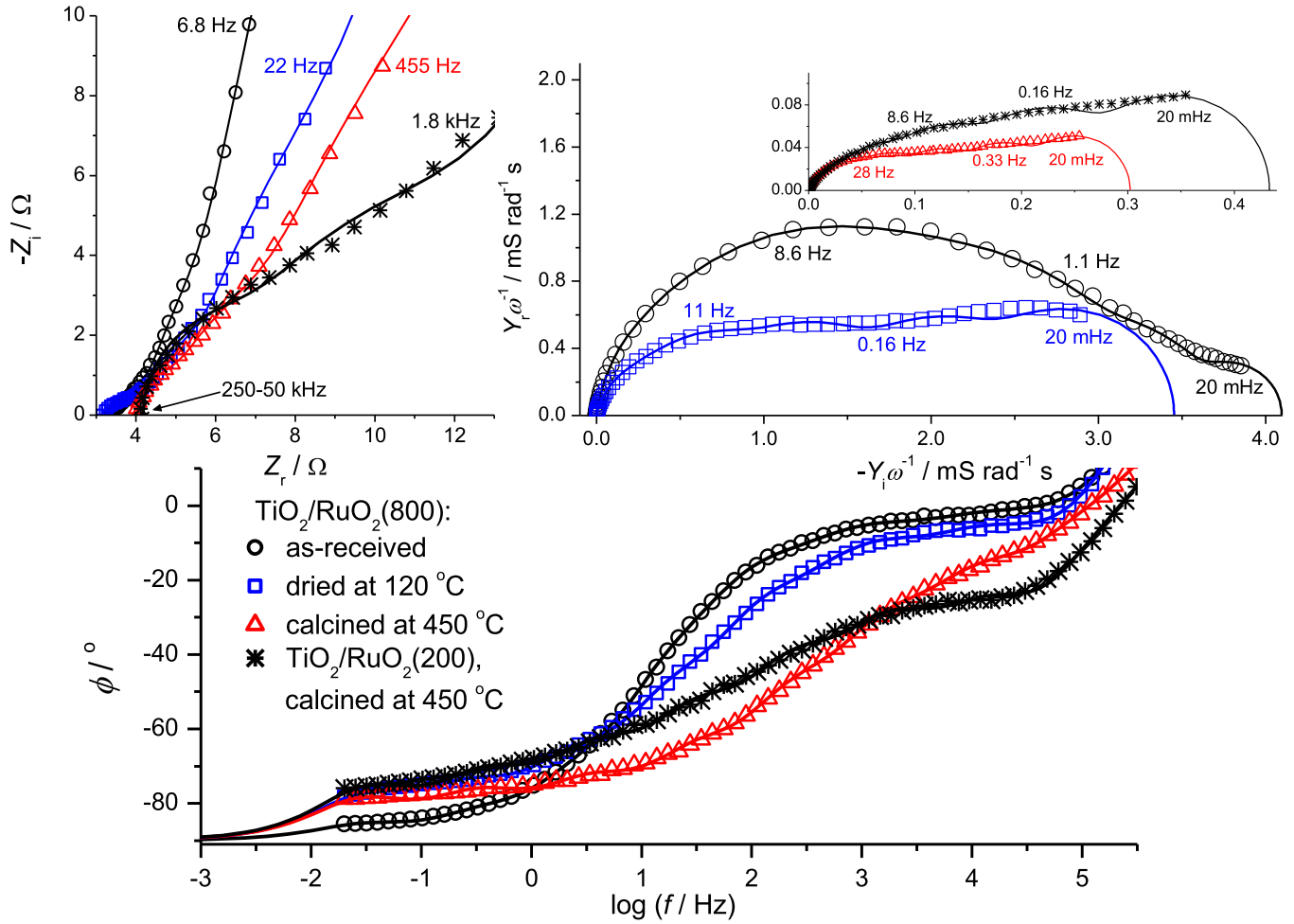

Figure 2. Registered (symbols) and fitting (lines) EIS data of the TiO_2/RuO_2 powders, USP-synthesized at 200 and 800°C. EIS data were recorded at the open circuit potential in 1.0 M H_2SO_4.

differences in activities of the corresponding coatings, Fig. 1, thus indicate the influence of the Ti support on the coating properties, which requires resolution. However, some differences in the powder properties could explain the unusual differences in surface mass compositions and the nominal one (3:2 RuO_2:TiO_2 for TiO_2/RuO_2(800), 2:3 for TiO_2/RuO_2(200) and 1:3 nominal[26]) and therefore they strengthen the impression of the core/shell hierarchy of the USP synthesized spheres.

As in the case of the drying effect, there is a mutual exchange point in the distributions, now at $n = 3$ when distributions for TiO_2/RuO_2(800) and TiO_2/RuO_2(200) are compared. The capacitance of the TiO_2/RuO_2(800) sample, rich in RuO_2 at the surface, is higher for $n < 3$, and lower for $n > 3$ in comparison to TiO_2/RuO_2(200) sample. The opposite is true for R_p for the reasons discussed in the preceding paragraphs. This apparently could be due to higher RuO_2 surface content, i.e., to RuO_2 content distribution from the sphere surface toward its interior. At higher USP temperature, the sphere surface is enriched more in RuO_2, due to the complete formation of separate oxide phases and the less pronounced migration in the solid phase throughout the sphere. The initial USP core/shell-generating stage is the encapsulation of the TiO_2 core by RuO_xH_y. During the pyrolysis, the core and the shell material grow into each other with their boundary being less defined as the synthesis temperature is lower. As a result of the generated core/shell hierarchy, the surface composition of both TiO_2/RuO_2(800) and TiO_2/RuO_2(200) is in favor of RuO_2 in-shell/TiO_2 in-core enrichment with respect to nominal composition.

Relations between the powder and coating dynamic responses and the mechanism of the activity loss of the coatings.—The registered dynamic responses (Fig. 3) of the calcined powders and corresponding coatings were found to be different.[26] The R_p values in the interior of the powders (i.e., sphere shell) for $n = 6$ and 7 are considerably higher than the corresponding values for the coatings, while the capacitances, i.e., the active sites of the initial powder, are located more in the interiors of the TiO_2/RuO_2(800) coating. On the contrary, the active sites are distributed uniformly within the TiO_2/RuO_2(200) coating. This uniform distribution could improve the stability[26] considerably, but does not promote the OER and CER activity (Fig. 1). The additional influence of the Ti support and coating formation reflects an increase of the total specific capacitance in comparison to the powders. This increase is also different for different synthesis temperatures: a six-fold increase was found for TiO_2/RuO_2(800) and three-fold for the TiO_2/RuO_2(200) coating.

The changes in voltammetric behavior caused by AST are presented in Fig. 4. As expected, the voltammetric charge is considerably decreased by AST. The decrease is the most pronounced for TiO_2/RuO_2(800), which was also found to be the least stable.[26] Its voltammetric response is much more resistive than capacitive, with almost complete exhaustion of the active material. The resistance of the spent TiO_2/RuO_2(800)/Ti and TiO_2/RuO_2(800cc)/Ti anodes is higher since their voltammograms are more tilted with respect to the TiO_2/RuO_2(200) anode. The shell-modified composition in the TiO_2/RuO_2(800cc)/Ti anode improves the stability,[26] while some active material is still present in a higher extent upon AST.

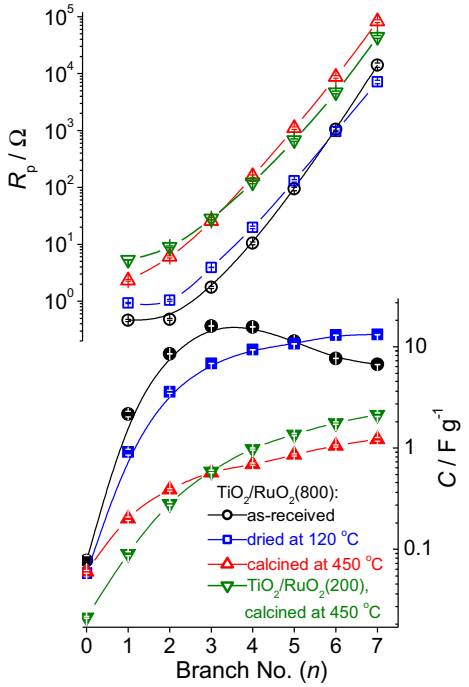

Figure 3. The pore resistance (R_p) and capacitance (C) distribution throughout the porous structure of USP powders synthesized at different temperatures. The values were obtained by fitting the data from Fig. 2 to a 7-branched transmission line equivalent electrical circuit (the error bars, all within the symbol size, represent standard deviation of the fitting data).

Further discussion of the AST-induced changes in the electrochemical properties of a coating and the correlation with the coating structure-caused activity/stability performances was derived from EIS-TLEEC data analysis. The registered EIS data as complex plane and Bode plots registered in the as-prepared state of the coatings (before AST) and after AST are shown in Fig. 5. In order to gain insight into the differences in EIS behavior in the solutions for OER and CER polarizations (Fig. 1), the EIS data were also recorded in NaCl solution. The differences in the EIS responses in the two solutions are rather negligible, whereas TiO_2/RuO_2(200)/Ti appeared as the least sensitive to the solution composition. The other two coatings, exhibiting lower capacitances and pore resistances,[26] showed some sensitivity in the mid- to low-frequency region, which will be discussed in relation to the resistance and the capacitance distributions (Fig. 6).

The main feature of the EIS data of the exhausted coatings is the declination of the spectrum in the complex plane toward the real impedance axis, with the accompanied appearance of a phase shift peak in the high frequency domain. In the cases of anodes with a similar surface composition, TiO_2/RuO_2(200)/Ti and TiO_2/RuO_2(800cc)/Ti, the peak relates to the appearance of a high frequency semicircle. For the anode of lowest stability,[26] TiO_2/RuO_2(800)/Ti, the peak appears over a much wider frequency range and relates to several overlapping loops in the complex plane. Exclusively for this anode, the peak is closely related to the one observed for the as-synthesized coating in the 1–10 kHz range. This initial peak is much better resolved in NaCl solution (higher pH) than in H_2SO_4. This finding indicates the presence of the coatings parts with hindered approach to the active sites, which are initial weak points for AST destabilization.

The appearance of the high-frequency semicircle is typical for exhausted DSA-type coatings.[13,40] The associated resistance, i.e., the diameter of the semicircle, was independent on the anode potential, and hence is electrical in nature. It was ascribed to the definite TiO_2-rich layer of very low conductance within the exhausted coating.

The proposed mechanisms for the loss of coating activity recognize two distinct origins of the layer.[25] There is surface enrichment of the coating with TiO_2 as RuO_2 electrochemically dissolves during the AST, but also the continuous growth of the TiO_2-rich layer in the coating/Ti support interphase. Although the loss of the conducting pathways is well registered from the coating dynamic responses by CV (decreased charge and the tilt, Fig. 4) or EIS (e.g., high-frequency semicircle, Fig. 5), the different origins of the layer, as well as their relation to the coating structure, can hardly be diagnosed. Presented here is the TLEEC approach to EIS data as a useful tool for registering differences among the competing mechanisms for the loss of activity.

A comparison of the pore resistance and the capacitance distribution within the synthesized coatings in their active[26] and inactive states is given in Fig. 6.

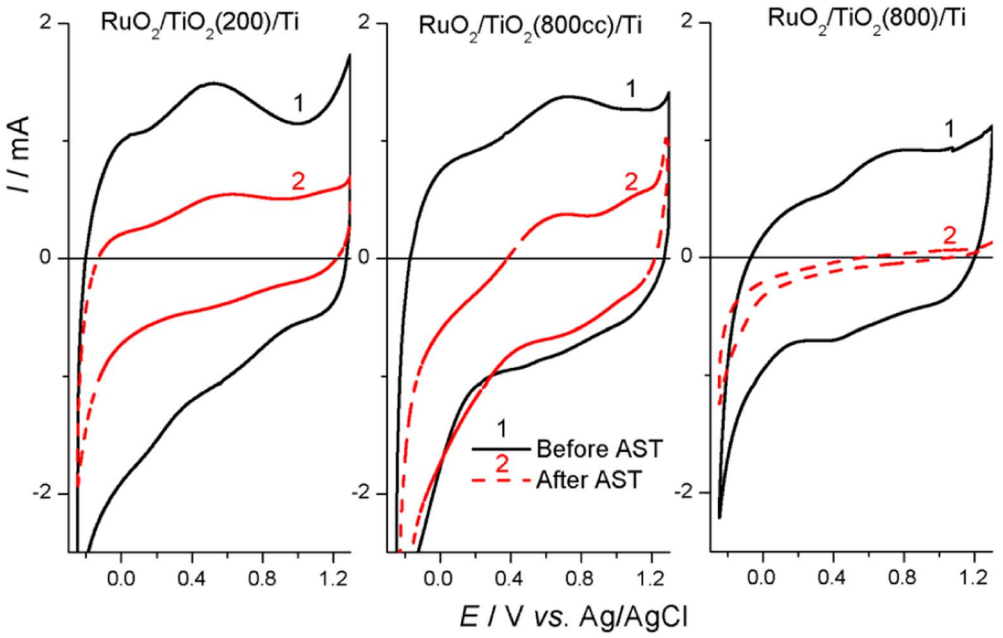

Figure 4. Cyclic voltammograms of USP-synthesized coatings on Ti recorded before and after the accelerated stability test (AST); 1.0 M H_2SO_4, $\nu = 50$ mV s^{-1}.

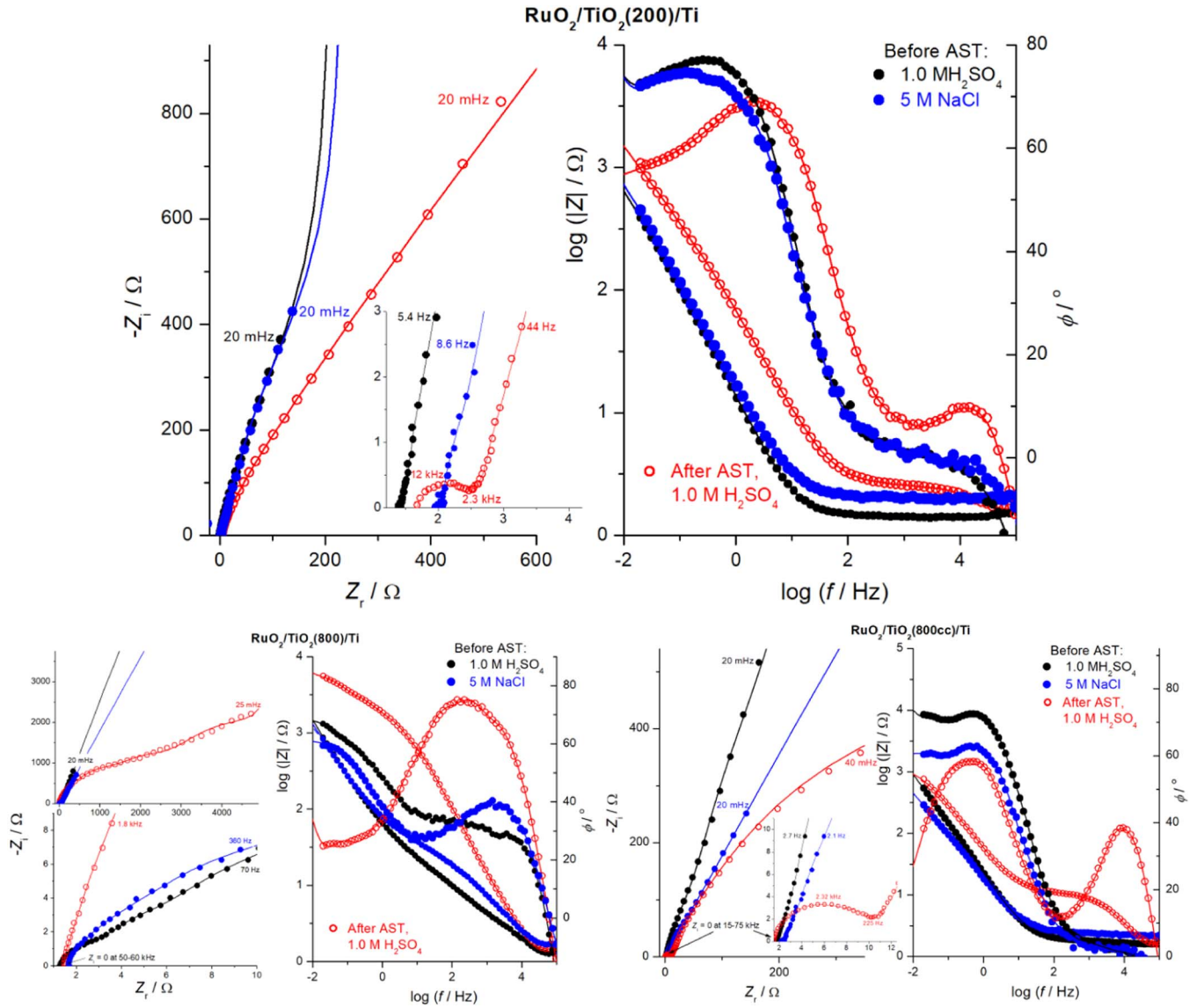

Figure 5. EIS plots of the data (symbols) of USP-synthesized coatings on Ti obtained before and after an accelerated stability test (AST) and in 1.0 M H_2SO_4 and 5 M NaCl (pH 2). The data of the corresponding TLEECs are presented by lines.

The distributions presented in Fig. 6 bring at least two unexpected and unusual features. As discussed, the loss of the activity is caused by the exhaustion of active sites and the appearance of low-conductivity zones and layers of definite thickness, which consequently induce an increase in the coating resistance. In AST, it causes a sudden increase in the anode potential as an indication of the inactive state of the coating. This should cause an overall increase in the EIS-related distributed coating resistance, if R_p relates to the resistance of the TiO_2-rich layer and the pseudocapacitive charge transfer resistance, as considered in relation to the distributions influenced by thermal treatments of the powders (Fig. 3). On the other hand, the pore resistance, assumed as the main constituent of the distributed resistance of the coating in its active state, should decrease due to exhaustion. The data for the coatings obtained at the higher USP temperature appear to follow the expectation of increased resistance upon deactivation. However, the values of the distributed resistance of the inactive TiO_2/RuO_2(200) beyond the first branch of TLEEC are considerably lower than in the active state, and even decrease as the capacitances from the corresponding branches increase in the external part of the coating (e.g., for $n = 1$ and 2). The likely trend was also seen for the TiO_2/RuO_2(800cc) coating that is of similar shell composition obtained by adjustment. This similarity in trends indicates that the mechanism of the activity loss for these two coatings was similar. The trend was, however, contrary for the TiO_2/RuO_2(800) coating.

In order to resolve the different resistance contributions to R_p, and consequently, the increase in the AST anode potential, the pore and capacitance distributions in different electrolytes were compared. The ohmic resistance of the NaCl solution was found to be higher than that of the H_2SO_4 solution in all EIS measurements. The distributed pore resistances should be higher too, but this was observed only for TiO_2/RuO_2(800) coating. For TiO_2/RuO_2(200) and TiO_2/RuO_2(800cc) coating, the resistances in NaCl were lower; at the external parts of the coating for the former, and at the internal for the later. Consequently, neither resistances for $n = 1$ (TiO_2/RuO_2(800cc)) and 5 (TiO_2/RuO_2(200)) nor the corresponding capacitances were "sensitive" to the electrolyte composition. On the other hand, both the pore and charge transfer resistances were functions of the solution conductivity and of pH, respectively. The insensitive resistances of the outer layers of TiO_2/RuO_2(800cc) and inner ones of TiO_2/RuO_2(200) are to be assigned to the considerable portion of non-conductive pathways among the mixed oxide spheres. These loose sphere boundaries are the coating weak points, liable to the growth of a finite TiO_2-rich

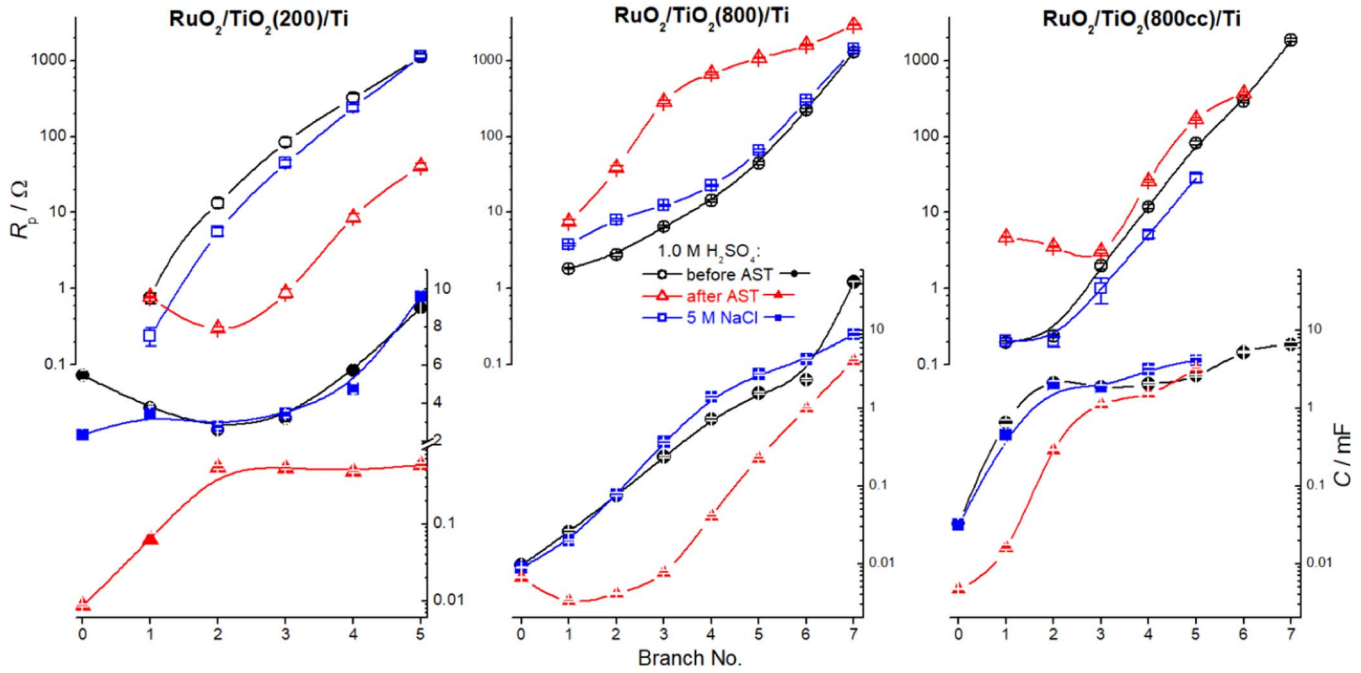

Figure 6. The pore resistance (R_p) and capacitance (C) distribution throughout the porous structure of USP-synthesized coatings on Ti. The values were obtained by fitting the data from Fig. 5 to a transmission line equivalent electrical circuit (the error bars, all within the symbol size, represent standard deviation of the fitting data).

layer during exhaustion of the active component in AST. In the case of the $TiO_2/RuO_2(800)$ coating, the "insensitivity" is differently distributed: the outer capacitances ($n < 3$) do not "feel" the electrolyte type, while the insensitive resistance is, similar to $TiO_2/RuO_2(200)$ coating, placed in the last branch of TLEEC. The stability-related weak point of the $TiO_2/RuO_2(200)$ coating hence relates rather to the pore resistance, and the capacitance insensitivity is caused by the very low values even up to $n = 4$. Consequently, the values of the capacitances for $n > 4$ is lower in NaCl than in H_2SO_4 due to the higher pH value.

In the further discussion of the changes with AST and the mechanisms of the activity loss, the following consideration could be meaningful. The preceding discussions related to the external and the internal parts of the coating, and their association to low and high n values of TLEEC consider the distribution in the space domain. However, the distributions relate also to the time domain. Namely, EIS data of low RC constants belong to the high frequency domain, and should not, as a rule, be related to the external parts of the coating. It was shown[13] that the EIS response of TiO_2-rich layers appears always in the high frequency domain. The corresponding data in Fig. 6 should therefore be found for n values related to the lowest values of the capacitances. The resistance for $n = 1$ is similar for the 800°C samples, around 10 Ω, while near 1-Ω resistance is found for $TiO_2/RuO_2(200)$. Roughly, these are also the diameters of the high frequency semicircles in the cases of $TiO_2/RuO_2(800cc)$/Ti and $TiO_2/RuO_2(200)$/Ti. The resistance of 10 Ω should increase the cell voltage by at least 10 V (for 1 A in AST), which is near the value for the diagnosis of the dysfunction of all anodes in AST.[26] In the case of $TiO_2/RuO_2(200)$/Ti, 1 Ω of resistance is not enough for inactivity and hence this anode is able to operate with the uniformly distributed internal active sites for n in range 2–5 behind additional 10 Ω of resistance of the widened pores. However, these active sates are behind the pores filled by gas and can consequently suddenly become inactive. A considerably greater number of internal active sites remained in the 800°C samples, but they are available beyond several hundreds and thousands of ohms and therefore, could not be active even under moderate polarizations. The non-availability of the internal active sites is apparently caused by the exhaustion of the already small number of external active sites without significant changes in the porous structure of the $TiO_2/RuO_2(800)$ sample. This should be recognized as the most probable mechanism for the activity loss of $TiO_2/RuO_2(800)$/Ti. On the other hand, owing to low initial external resistances of $TiO_2/RuO_2(800cc)$ and $TiO_2/RuO_2(200)$ coatings, associated with wide coatings cracks,[26] the growth of a TiO_2-rich layer in the coating/substrate interphase is more probable. For $TiO_2/RuO_2(200)$/Ti, characterized by considerable greater number of external active sites, working potential of AST should be considerably lower, and therefore the growth of a layer is much slower. At the end of AST, the corresponding resistance (around 1 Ω, $n = 1$) is considerably lower than for $TiO_2/RuO_2(800cc)$/Ti (around 10 Ω, $n =$ 1 and partially 2). Consequently, the inactive $TiO_2/RuO_2(800cc)$/Ti suffers from a rapid increase in the resistance by 10 Ω in the interphase, whereas some portion of the active sites are available behind at least 10 Ω pore resistance for the inactive $TiO_2/RuO_2(200)$/Ti. Hence, $TiO_2/RuO_2(200)$/Ti loses activity after a considerably longer time in AST.

It follows that the analysis of the resistance and the capacitance distributions of the coatings in the active and inactive state is able to explain the causes of the loss of coating activity and to correlate these causes with the different coating structures.

Conclusions

The unique dependence of the activity of TiO_2/RuO_2 coatings on Ti for the oxygen and chlorine evolution reactions (OER and CER, respectively) on the temperature of the ultrasonic spray pyrolysis (USP) synthesis was considered in relation to the observed stabilities of the coatings in an accelerated stability test (AST). Two USP temperature extremes were subjected to investigation, 200 and 800°C.

The electrochemical properties of the synthesized TiO_2/RuO_2 microspheres indicate their core/shell-like structure from their dynamic responses, with different distributions of RuO_2, the active component, through the shell. The different shell structures appeared responsible for the differences in OER and CER activities, which were found superior for the 800°C sample. However, the opposite was valid for the stability – the 200°C sample was considerably more stable.

Cyclic voltammetry showed the usual relationship between the coatings in their active and inactive states. The decrease in voltammetric charges and in the coating resistances were both more pronounced for the 800°C sample.

The transmission line equivalent electrical circuit (TLEEC) was applied for analysis of the electrochemical impedance spectroscopic (EIS) responses of the USP powders and coatings. The analysis enabled the elucidation of the resistance and the capacitance distributions in time (down the TLEEC) and the space domain (through the powder layers and coating). The different compositions of the sphere shell were reflected in the distributions. The capacitance was more uniformly distributed within the 200°C sample of lower surface RuO_2 composition. The resistance distribution indicated the contributions of pore and pseudocapacitive charge transfer resistance. The distributions for the USP powders that were thermally treated indicated the distribution of the hydration degree through the spherical particles. The capacitance of the powders was consequently considerably decreased by the drying and calcinations of the powders.

The different stabilities of the coatings prepared at different USP temperatures were considered from an analysis of the changes in the resistance and the capacitance distributions. The 800°C sample suffered from the fast exhaustion of RuO_2 from the coating surface, while the adjustment of the surface composition by the additional TiO_2 at the sphere surface improved the stability only negligibly, because the adjustment favored the growth of a TiO_2-rich layer at the coating/Ti substrate interphase. This growth was also registered for the 200°C sample, but the real cause of the loss of its activity is the uniform exhaustion of RuO_2 throughout the coating. For all samples, the end of coating service life was indicated by the increase in the coating resistance, due to an increase in the pore resistance (200°C sample) or a rise in the resistance of loose grain boundaries (800°C sample).

Acknowledgment

M.K., N.V., and V.P. acknowledge the financial support by the Ministry of Education, Science and Technological Development of the Republic of Serbia (MESTDRS), Contract No. 172060. Part of the research was supported by the funds of the bilateral research project, ID 451-03-01413/2016-09/7, supported by Deutsche Akademische Austausch Dienst (DAAD), Germany, and MESTDRS. To Prof. Radoslav Adzic for his huge and long-lasting contribution to contemporary electrochemistry.

ORCID

Vladimir Panić https://orcid.org/0000-0002-8358-7956

References

1. J. Jiang, Y. Li, J. Liu, X. Huang, C. Yuan, and X. W. Lou, Recent advances in metal oxide-based electrode architecture design for electrochemical energy storage, *Adv. Mater.*, **24**, 5166 (2012).
2. J. Hu, L. Wu, K. A. Kuttiyiel, K. Goodman, C. Zhang, Y. Zhu, M. Vukmirovic, M. G. White, K. Sasaki, and R. R. Adzic, Increasing Stability and Activity of Core–Shell Catalysts by Preferential Segregation of Oxide on Edges and Vertexes: Oxygen Reduction on Ti–Au@Pt/C, *J. Am. Chem. Soc.*, **138**, 9294 (2016).
3. K. Sasaki, H. Naohara, Y. Cai, Y. M. Choi, P. Liu, M. B. Vukmirovic, J. X. Wang, and R. R. Adzic, Core-protected platinum monolayer shell high-stability electrocatalysts for fuel-cell cathodes, *Angew. Chem. Int. Ed.*, **49**, 8602 (2010).
4. K. Sasaki, H. Naohara, Y. M. Choi, Y. Cai, W.-F. Chen, P. Liu, and R. R. Adzic, Highly stable Pt monolayer on PdAu nanoparticle electrocatalysts for the oxygen reduction reaction, *Nature Commun.*, **3**, 1115 (2012).
5. A. Kowal, M. Li, M. Shao, K. Sasaki, M. B. Vukmirovic, J. Zhang, N. S. Marinkovic, P. Liu, A. I. Frenkel, and R. R. Adzic, Ternary Pt/Rh/SnO_2 electrocatalysts for oxidizing ethanol to CO_2, *Nature Mater.*, **8**, 325 (2009).
6. K. Sasaki, K. A. Kuttiyiel, J. X. Wang, M. B. Vukmirovic, and R. R. Adzic, in *Electrocatalysts for Low Temperature Fuel Cells: Fundamentals and Recent Trends*, T. Maiyalagan and V. S. Saji, Editors, p. 557, Wiley-VCH, Weinheim (2017)
7. S. Trasatti, Electrocatalysis: Understanding the Success of DSA, *Electrochim. Acta*, **45**, 2377 (2000).
8. X. Wang and R. Gordon, High-Quality Epitaxy of Ruthenium Dioxide, RuO_2, on Rutile Titanium Dioxide, TiO_2, by Pulsed Chemical Vapor Deposition, *Cryst. Growth Des.*, **13**, 1316 (2013).
9. S. Ferro, M. Donatoni, A. De Battisti, and V. N. Andreev, Adsorption of Thallium Cations on RuO_2–TiO_2 Electrodes, *J. Appl. Electrochem.*, **37**, 1389 (2007).
10. V. Panić, A. Dekanski, S. Milonjić, V. Mišković-Stanković, and B. Nikolić, Electrocatalytic activity of sol-gel-prepared RuO_2/Ti anode in chlorine and oxygen evolution reactions, *Russ. J. Electrochem.*, **42**, 1055 (2006).
11. C. Hu, H. Guo, K. Chang, and C. Huang, Anodic composite deposition of $RuO_2 \cdot xH_2O$–TiO_2 for electrochemical supercapacitors, *Electrochem. Commun.*, **11**, 1631 (2009).
12. V. Panić, A. Dekanski, and R. Stevanović, Sol–gel processed thin-layer ruthenium oxide/carbon black supercapacitors: A revelation of the energy storage issues, *J. Power Sources.*, **195**, 3969 (2010).
13. V. Panić, A. Dekanski, V. Mišković-Stanković, S. Milonjić, and B. Nikolić, On the deactivation mechanism of RuO_2–TiO_2/Ti anodes prepared by the sol–gel procedure, *J. Electroanal. Chem.*, **579**, 67 (2005).
14. Y. Wang, Z. Wang, and Y. Xia, An asymmetric supercapacitor using RuO_2/TiO_2 nanotube composite and activated carbon electrodes, *Electrochim. Acta*, **50**, 5641 (2005).
15. M. Aparicio and L. Kleint, Thin and Thick RuO_2-TiO_2 Coatings on Titanium Substrates by the Sol-Gel Process, *J. Sol-Gel Sci. Technol.*, **29**, 81 (2004).
16. D. Suh, T. Park, W. Kim, and I. Hong, Synthesis of high-surface-area ruthenium oxide aerogels by non-alkoxide sol–gel route, *J. Power Sources*, **117**, 1 (2003).
17. B. Yao, L. Wang, C. Wang, Z. Wang, and G Yhao, Preparation and Performances of RuO_2/TiO_2 Films Photocatalyst Supported on Float Pearls, *Chin. J. Chem. Phys.*, **20**, 789 (2007).
18. C. C. Hu, K. H. Chang, M. C. Lin, and Y. T. Wu, Design and Tailoring of the Nanotubular Arrayed Architecture of Hydrous RuO_2 for Next Generation Supercapacitors, *Nano Lett.*, **6**, 2690 (2006).
19. Y.-G. Wang and X.-G Zhang, Preparation and electrochemical capacitance of RuO_2/TiO_2 nanotubes composites, *Electrochim. Acta*, **49**, 1957 (2004).
20. Y. Xie, L. Zhou, C. Huang, Y. Liu, and J. Lu, Preparation and electrochemical capacitance of ruthenium oxide-titania nanotube composite, *Mater. Sci. Forum*, **614**, 235 (2009).
21. Z. Ma, Y. Zhang, S. Liu, W. Xu, L. Wu, Y.-C. Hsieh, P. Liu, Y. Zhu, K. Sasaki, J. N. Renner, K. E. Ayers, R. R. Adzic, and J. X. Wang, Reaction mechanism for oxygen evolution on RuO_2, IrO_2, and RuO_2@IrO_2 core-shell nanocatalysts, *J. Electroanal. Chem.*, **819**, 296 (2018).
22. S. Stopić, B. Friedrich, M. Schroederm, and T. Weirich, Synthesis of TiO_2 core/RuO_2 shell particles using multi step ultrasonic spray pyrolysis, *Mater. Res. Bull.*, **48**, 3633 (2013).
23. M. Košević, S. Stopic, A. Bulan, J. Kintrup, R. Weber, J. Stevanović, V. Panić, and B. Friedrich, A continuous process for the ultrasonic spray pyrolysis synthesis of RuO_2/TiO_2 particles and their application as a coating of activated titanium anode, *Adv. Powder Technol.*, **28**, 43 (2017).
24. J. C. Forti, P. Olivi, and A. De Andrade, Characterisation of DSA®-type coatings with nominal composition $Ti/Ru_{0.3}Ti_{(0.7-x)}Sn_xO_2$ prepared via a polymeric precursor, *Electrochim. Acta*, **47**, 913 (2001).
25. V. M. Jovanovic, A. B. Dekanski, P. Despotov, B. Z. Nikolic, and R. T. Atanasoski, The roles of the ruthenium concentration profile, the stabilizing component and the substrate on the stability of oxide coatings, *J. Electroanal. Chem.*, **339**, 147 (1992).
26. M. Košević, S. Stopic, V. Cvetković, M. Schroeder, J. Stevanović, V. Panić, and B. Friedrich, *Appl. Surface Sci.*, **464**, 1 (2019).
27. Z. Yi, C. Kangning, W. Wei, J. Wang, and S. Lee, Effect of IrO_2 loading on RuO_2–IrO_2–TiO_2 anodes: A study of microstructure and working life for the chlorine evolution reaction, *Ceram. Int.*, **33**, 1087 (2007).
28. V. Panić, A. Dekanski, S. Milonjić, R. Atanasoski, and B. Nikolić, The influence of the aging time of RuO_2 and TiO_2 sols on the electrochemical properties and behavior for the chlorine evolution reaction of activated titanium anodes obtained by the sol-gel procedure, *Electrochim. Acta*, **46**, 415 (2000).
29. B. Conway, *Electrochemical Supercapacitors – Scientific Fundamentals and Technological Applications*, Plenum Publishers, New York (1999).
30. B. Pillay and J. Newman, *J. Electrochem. Soc.*, **143**, 1806 (1996).
31. T. Liu, W. G. Pell, and B. E. Conway, *Electrochim. Acta*, **42**, 3541 (1997).
32. A. Lasia, *Electrochemical impedance spectroscopy and its applications*, pp. 203, Springer, New York (2014).
33. G. Šekularac, M. Košević, A. Dekanski, V. Djokić, M. Panjan, and V. Panić, High Energy/Power Supercapacitor Performances of Intrinsically Ordered Ruthenium Oxide Prepared through Fast Hydrothermal Synthesis, *ChemElectroChem*, **4**, 2535 (2017).
34. B. Ž. Nikolić and V. Panić, in *Encyclopedia of Applied Electrochemistry*, G. Kreysa, K.-I. Ota, and R. F. Savinell, Editors, p. 411, Springer, New York (2014).
35. R. L. Doyle and M. E. G. Lyons, in *Photoelectrochemical Solar Fuel Production: From Basic Principles to Advanced Devices*, S. Giménez and J. Bisquert, Editors, Springer, Basel (2016).
36. Y.-H. Fang and Z.-P. Liu, Mechanism and Tafel lines of electro-oxidation of water to oxygen on RuO_2(110), *J. Am. Chem. Soc.*, **132**, 18214 (2010).
37. S. Trasatti, in *Interfacial Electrochemistry – Theory, Experiment and Applications*, A. Wieckowski, Editor, p. 769, Marcel Dekker Inc., New York (1990).
38. L. Birry and A. Lasia, *J. Appl. Electrochem.*, **34**, 735 (2004).
39. S. Ardizzone and S. Trasatti, Interfacial properties of oxides with technological impact in electrochemistry, *Adv. Colloid Interface Sci.*, **64**, 173 (1996).
40. C. L. P. S. Zanta, A. R. de Andrade, and J. F. C Boots, Solvent and support electrolyte effects on the catalytic activity of Ti/RuO_2 and Ti/IrO_2 electrodes: oxidation of isosafrole as a probe model, *Electrochim. Acta*, **44**, 3333 (1999).